



WILLIAMSON FLUID FLOW AND HEAT TRANSFER ANALYSIS OVER A STRETCHED SHEET ALONG WITH NEWTONIAN HEATING IN THE EXISTENCE OF THERMAL RADIATIVE, BUOYANCY, AND VISCID DISSIPATIVE IMPRESSION

SANJU JANGID¹, RUCHIKA MEHTA¹ and MANOJ KUMAR SHARMA²

¹Department of Mathematics and Statistics
Manipal University Jaipur
Jaipur (Raj.), India
E-mail: ruchika.mehta1981@gmail.com

²Department of CCE
Manipal University Jaipur
Jaipur (Raj.), India

Abstract

Thermal radiative and viscid dissipative impression of non-Newtonian Williamson fluid is analysed over a stretched sheet with the magnetic field, Newtonian heating, and buoyancy force. With the help of some similarity transformative terms, the governing equation (dimensional partial differential equations) is converted into non-dimensional ordinary differential equations and solved by the bvp4c method. The current study discovered the momentum and temperature impressions of many non-dimensional physical parameters in graphs and tables with the help of MATLAB software. Validations of complete situations for a specific condition have been completed, and a very actual arrangement has been touched.

1. Introduction

Extrusion processes rely heavily on fluid dynamics induced by stretching sheets. The non-Newtonian fluid has progressed, according to a recent study. A study of non-Newtonian can track this expansion using the characteristics of the liquid employed in many technology and construction operations such

2020 Mathematics Subject Classification: 76S05, 76D05, 65L06.

Keywords: viscous dissipation, thermal radiation, aligned angle, Williamson fluid, bvp4c.

Received July 7, 2022; Accepted December 12, 2022

as polymeric surface manufacturing, continuous casting, paper production, and aeronautical extrusive of plastic sheets.

Salleh et al. [17] studied the time-independent heat transfer of non-Newtonian Williamson fluid flow over a stretched sheet along with Newtonian heating. Mohamed et al. [12] examined the mathematical explanation of stagnation point flow across a stretch sheet caused by Newtonian heating. The heat transference from the sheet is equivalent to the local sheet temperature. In the presence of Newtonian heating, Qasim et al. [15] investigated the Micropolar fluid constant flow across a stretched sheet with heat transmission. Finally, Sarif et al. [18] investigated time-independent heat transmission features across a stretched surface with Newtonian heating. Heat transference from the sheet is equivalent to the local surface temperature. In the presence of Newtonian heating, Ramzan and Yousaf [16] explored continuous 3D boundary layer viscoelastic nanofluid flow. Das et al. investigated [5] the hydromagnetic boundary layer slipping flow across a stretched surface in nanofluid along with Newtonian heating in the appearance of a uniform transverse magnetic impression, thermal radiative, and 1st-order chemical reaction in the existence of a universal transverse magnetic field, thermal radiation, and first-order chemical reaction.

Devi and Devi [6] investigated the impacts of Lorentz force across a 3D stretched sheet subjected to Newtonian heating along with thermo-physical features by comparing the heat transference characteristics of classic nanofluid with those of emergent hybrid nanofluid. Boundary layer flow and heat transmission on casson fluid with dust particles across a stretched surface were numerically discovered by Arifin et al. [3]. In Arifin's problem, the effects of an aligned magnetic field combined with Newtonian heating are considered. Ullah et al. [19] explore the role of the slip-on hydromagnetic free convective non-Newtonian fluid flow across a non-linearly stretched surface immersed in porous media with Newtonian heating. In the presence of Newtonian heating, Rahman et al. [20] explored the role of homogeneous/heterogeneous interactions on the flow and heat transference of customized second-grade fluid across a non-linearly stretched sheet. Arifin et al. [2] study the influence of an aligned magnetic field in a mixed convective of dusty Casson fluid across a stretched sheet numerically. Bing et al. [4]

researched the boundary layer hydromagnetic Williamson nanofluid flow across a stretched sheet along with Newtonian heating and thermal radiative impact. The hydromagnetic Casson fluid flow and heat transference to a non-linearly extending sheet with Newtonian heating were addressed by Hussanan et al. [9]. The influences of homogeneous/heterogeneous interactions on electrically conducted boundary layer fluid flow and heat transference properties across a stretched surface with Newtonian heating were researched by Khan et al. [10].

Ahmad et al. [1] study a time-independent 2D boundary layer flow and heat transference of a Casson fluid across a stretching plate with a Newtonian heating flow state. Thermal radiative influences on hydromagnetic stagnation point flow of shear thinning Williamson fluid across a stretched sheet were examined by Hashim et al. [8]. Mohamed et al. [13] studied the flow and heat transmission of water-based magnetite (Fe_3O_4) nanofluid called ferrofluid across a stretched sheet with a slip effect. Goud et al. [7] used a stretching sheet with Newtonian heating to investigate the aligned magnetic field with shear-thinning Williamson fluid. Finally, Madhukesh et al. [11] used a non-Fourier heat flux model to study of the AA7072-AA7075/water-based hybrid nanofluid flow across a bent stretched sheet. Furthermore, heat transport is investigated under two boundary circumstances: Newtonian heating and unvarying wall temperature. The analytical simulation of a mixed convective of Walters-B nanofluid flow across a stretched surface with Newtonian heating and volume fraction due to the accessibility of magnetic impact and mass suction was examined by Qaiser et al. [14].

This research aimed to look at shear-thinning Williamson fluid flow with the appropriate Newtonian heating configuration, aligned magnetic impression, thermal radiative, buoyancy force, and viscous dissipative influences founded on the overhead works.

2. Formulation

The movement of shear-thinning Williamson fluid over a stretched surface with a stretched linear momentum $u_w(x) = ax$ is regarded as a steady, incompressible (density = constant) 2D boundary layer flow. The flow

is subjected to an aligned magnetic field with an acute angle ϕ , as shown in Figure 1.

Constitutional relations for non-Newtonian Williamson fluid are

$$S = -PI + \tau, \text{ here } \tau = \left(\mu_\infty + \frac{\mu_0 - \mu_\infty}{1 - \Gamma\beta} \right) A_1,$$

Where P positions for pressure, I expression for identity vector, τ suggestions the additional stress tensor, μ_0 and μ_∞ exhibition for limit viscosity at 0 and ∞ shear rate respectively, A_1 offerings the Rivilin-Erickson tensor and β is distinct as

$$\beta = \sqrt{\frac{1}{2}} \pi, \pi = \text{trace}(A_1)^2.$$

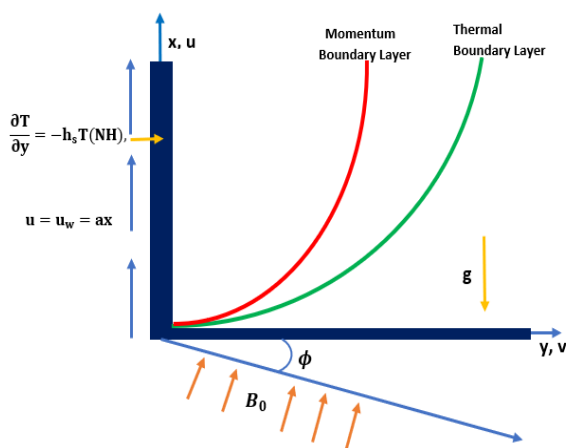


Figure 1. Schematic illustration.

The dimensional governing equations of current effort are decorated as tracks:

$$\frac{\partial u}{\partial x} + \frac{\partial v}{\partial y} = 0 \tag{1}$$

$$u \frac{\partial u}{\partial x} + v \frac{\partial u}{\partial y} = \nu \frac{\partial^2 u}{\partial y^2} + \sqrt{2}\Gamma v \frac{\partial u}{\partial y} \frac{\partial^2 u}{\partial y^2} + \sigma u \beta_0^2 (\sin \phi)^2 + g\beta_T(T - T_\infty) - \frac{\nu}{k'} u \tag{2}$$

$$\begin{aligned}
 u \frac{\partial T}{\partial x} + v \frac{\partial T}{\partial y} &= v \frac{\partial^2 T}{\partial y^2} - \frac{1}{\rho C_p} \frac{\partial q_r}{\partial y} \\
 &+ \frac{\mu}{\rho C_p} \left(1 + \frac{\Gamma}{\sqrt{2}} \frac{\partial u}{\partial y} \right) \left(\frac{\partial u}{\partial y} \right)^2 \frac{Q_0}{\rho C_p} (T - T_\infty) - \frac{v}{k} u
 \end{aligned}
 \tag{3}$$

The associatory limitations are

$$\begin{aligned}
 u &= u_w(x) = ax, v = 0, \frac{\partial T}{\partial y} = -h_s T, \text{ at } y = 0 \\
 u &= 0, T \rightarrow T_\infty, \text{ at } y = \infty
 \end{aligned}
 \tag{4}$$

The momentum features u (m.s⁻¹) and v (m.s⁻¹) are located along the x and y axes, correspondingly. Moreover, ν (m².s⁻¹) is the kinematic viscosity, Γ denotes the time constant, σ exhibits the conductivity electricity field, β_0 (N.m.A⁻¹) signifies the magnetic field strength, ρC_p (J.m⁻³.K⁻¹) displays the heat capacity of nano-fluids, ϕ depicts the aligned angle parameter, T is the temperature of fluid, and h_s denotes the heat transmission coefficient, and α denotes the thermal diffusivity, ∞ indicates to the condition at the free stream.

The roseland guesstimate of the radiation heat flux is settled by

$$q_r = \frac{-4\sigma^*}{3k^*} \frac{\partial T^4}{\partial y}
 \tag{5}$$

Here T^4 as a linear connection of temperature through Taylor's arrangement extension about T_∞ and disregarding progressive terms, thus

$$T^4 \approx 4T_\infty^3 T - T_\infty^4
 \tag{6}$$

With the procedure of the under-mentioned similarity transformations

$$\eta = \sqrt{\frac{a}{\nu}} y, \psi = \sqrt{avx}, u = \frac{\partial \psi}{\partial y} = axf, v = -\frac{\partial \psi}{\partial x} = -\sqrt{avf},$$

and $\theta(\eta) = \frac{T - T_\infty}{T_\infty},$ (7)

Here η and $\theta(\eta)$ indicate dimensionless variables, respectively, and ψ is the stream operator.

The resulting results are obtained by inserting Equation (7) in Equations (2)-(3) and (4):

$$f''' = \{(f')^2 - ff'' + Mn(\sin\phi)^2 f' + k_2 f' - G_T \theta\} / (1 + wf'') \quad (8)$$

$$\theta'' = (-1) Pr \{f\theta' + Ec(1 + (W/2)f'')(f'')^2 + Q\theta\} / (1 + Nr) \quad (9)$$

and limitations are specified by

$$\begin{aligned} f(0) = 0, f'(0) = 1, \theta(0) = -\gamma(1 + \theta), \text{ at } \eta = 0 \\ f'(\infty) \rightarrow 0, \theta(\infty) \rightarrow 0, \text{ at } \eta \rightarrow \infty \end{aligned} \quad (10)$$

Where $W = \Gamma \sqrt{\frac{2a^3}{\nu}}$ defines the dimensionless Weissenberg parameter, $Mn = \frac{\sigma\beta_0^2}{a}$ shows the magnetic (Hartman) parameter, $k_2 = \frac{\nu}{ak'}$ describes the permeability parameter, $G_T = \frac{g_0\beta_T T_\infty}{a^2 x}$ describes the local temperature Grashof number, $Nr = \frac{16\sigma^* T_\infty^3}{3kk^*}$ displays the radiative impression, $Pr = \frac{\mu C_p}{k} = \frac{\nu}{\alpha}$ represents the Prandtl number, $Q = \frac{Q_0}{C_p \rho a}$ illustrates the heat source or sink parameter, $\gamma = h_s \sqrt{\frac{\nu}{a}}$ labels the Eckert parameter, and $\gamma = h_s \sqrt{\frac{\nu}{a}}$ represents a conjugate section for Newtonian heating. It should be distinguished that $\gamma = 0$ refers to the cloistered plate, as well as the fact that the sheet temperature does not fluctuate, i.e., stays unchanged.

The skin friction coefficient C_f which is providing by physical measures of notice is $C_f = \frac{\tau_w}{\rho u_w^2}$, and the Nusselt number is well-defined as

$$Nu_x = \frac{xq_w}{k}.$$

The surface shear stress τ_w is assumed by $\tau_w = \mu \left(\frac{\partial u}{\partial y} \left(1 + \frac{\Gamma}{\sqrt{2}} \frac{\partial u}{\partial y} \right) \right)_{y=0}$,

we get

$$C_f \text{Re}_x^{-1/2} = f''(0) + (W/2)(f''(0))^2,$$

and the Nusselt parameter (heat transfer coefficient) is allocated as

$$\text{Nu}_x \text{Re}_x^{-1/2} = -\theta'(0).$$

Where, $\text{Re}_x = \frac{xu_w}{\nu}$ is the Reynolds number.

3. Numerical Structure

Equations are solved via bvp4c technique and shooting method. All numerical values and graphs are found with MATLAB software which is discussed in through tables and graphs.

First, apply the shooting method as:

$$f = y(1), f' = y(2), f'' = y(3), \theta = y(4), \theta' = y(5).$$

Equations (11)-(14) reduce into newform as:

$$f''' = \{(y(2))^2 - y(1) * y(3) + Mn * (\sin\phi)^2 * y(2) + k_2 * y(2) - G_T * y(4)\} / (1 + W * y(3)) \quad (11)$$

$$\theta'' = (-1) * Pr * \{y(1) * y(5) + Ec * (1 + (W/2) * y(3)) * (y(3))^2 + Q * y(4)\} / (1 + Nr) \quad (12)$$

and limitations are specified by

$$y_0(1) = 0, y_0(2) = 1, y_0(5) = -\gamma * (1 + y_0(4)), \text{ at } \eta = 0$$

$$y_\infty(2) \rightarrow 0, y_\infty(4) \rightarrow 0, \text{ at } \eta \rightarrow \infty \quad (13)$$

To 10^{-5} , the border remained constant. The choice $\eta(\infty) = 3$ indicates that each numerical output approaches asymptotic assets ideally in this technique.

4. Result and Discussion

Williamson fluid over a stretched sheet with viscid dissipation and thermal conductivity is evaluated using the `bvp4c` technique. The findings are consistent with prior studies. The latest findings appear to be in line with the previous studies. The impact of multiple physical parameter values on momentum, temperature, volume fraction, skin-friction coefficient, and Nusselt parameter values gotten with MATLAB software is exposed in Figures 2-16 and Table 1. For current research, we measured the values of physical parameters as: $W = 0.1 = k_2 = G_T = Nr = Ec = Q$, $Mn = \gamma = 1$, $Pr = 7$, and $\phi = \pi/6$.

The effects of inflation Williamson parameters W on the momentum and temperature profiles are shown in Figure 2 and Figure 7, respectively. When the elasticity stress parameter improves, momentum decreases because the Williamson parameter produces more significant restrictions in fluid flow. Conversely, the temperature profile increases with the upsurge Williamson parameter. In addition, when the non-Newtonian Williamson parameter grows, the skin friction coefficient and heat transmission coefficient for Williamson fluid decrease. The expanding influence of the Hartman number Mn on the momentum and temperature profiles is seen in Figures 3 and 10. When Hartman parameter values are enhanced, velocity graphs are lowered due to an opposing force known as the Lorentz force. Because as Mn levels grow, fluid-particle mobility ceases and diffuses quickly to the boundary's neighbouring layers, the temperature outline exhibits a rising trend. In addition, the skin friction coefficient and heat transmission coefficient for Williamson fluid drop when the magnetic parameter Mn increases. The increasing momentum profile and the dropping temperature profile impacts of the increased local temperature Grashof number G_T are shown in Figures 5 and 9. The Grashof quantity represents the proportion of buoyancy to restricting force. The buoyant force is created by the standard deviation in the density of the fluid, and the restricting strength makes the liquid viscosity. In addition, when the local temperature Grashof parameter rises, the skin friction coefficient and heat transference coefficient for Williamson fluid decrease.

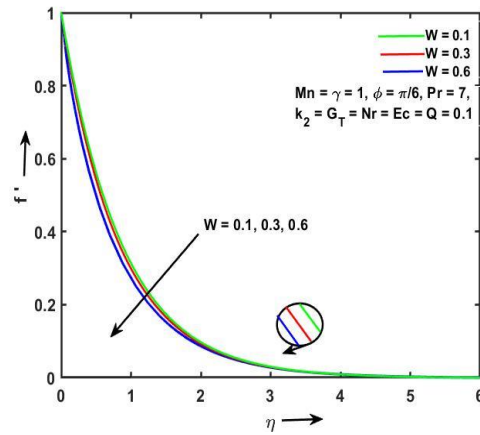


Figure 2. Momentum drawings for numerous W values.

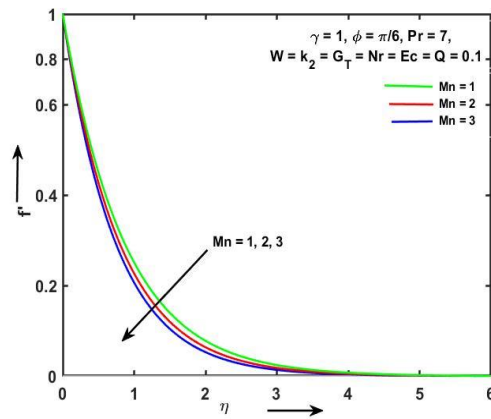


Figure 3. Momentum drawings for numerous Mn values.

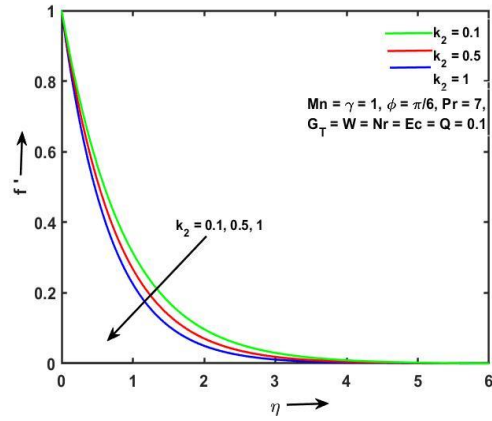


Figure 4. Momentum drawings for numerous k_2 values.

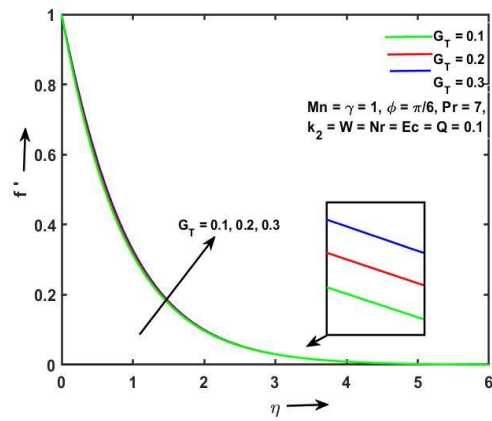


Figure 5. Momentum drawings for numerous G_T values.

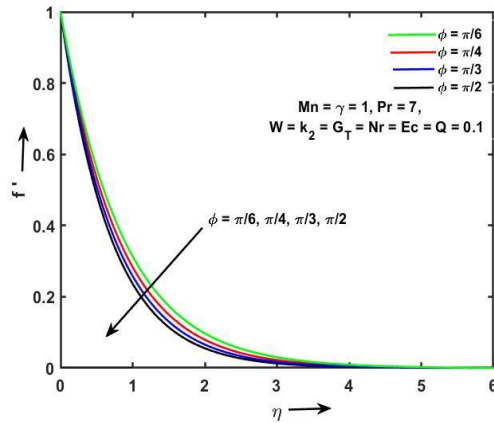


Figure 6. Momentum drawings for numerous ϕ values.

In Figures 4 and 8, the increasing permeability parameter k_2 decreases the velocity profile while enhancing the temperature profile. The skin friction coefficient and heat transmission coefficient for Williamson fluid also drop as the permeability parameter increases. Figures 6 and 15 show the effects of changing the aligned angle parameter (ϕ) on the velocity and temperature profiles, respectively. The significant findings are the alignment influence, which can range from $\pi/6$ to $\pi/2$, and where the magnetic impact is assumed to be absent by a value of 0. The velocity gradient has been demonstrated to diminish when the angle rises. And temperature graphs have been adjusted to climbing as the angle changes. As the alignment angle parameter increases, the skin friction coefficient and heat transmission coefficient for Williamson fluid decrease. Figure 12 describes the outcome of Prandtl on the temperature field for various Prandtl values. By reason of a high Pr-value, very viscid fluid with limited thermal conductivity is present as Pr values grow and diminish the temperature distribution. In terms of physics, the Prandtl amount is the relationship between velocity and thermal diffusivities; greater Pr amounts have lesser conduction, whereas lower Pr amounts have higher thermal conductivity. Therefore, as the Prandtl parameter increases, the skin friction coefficient decreases, and the heat transmission coefficient increases for Williamson fluid.

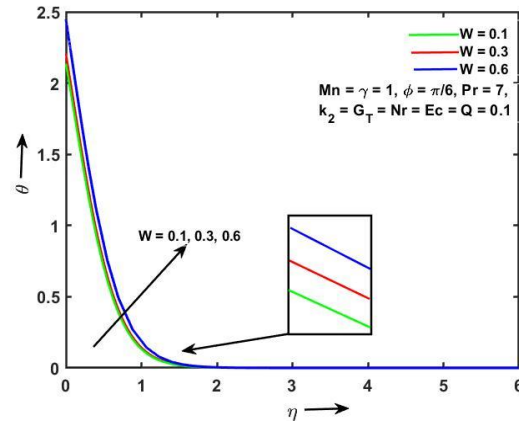


Figure 7. Temperature drawings for numerous W values.

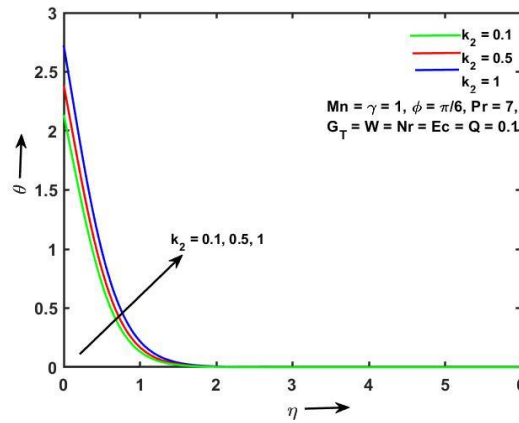


Figure 8. Temperature drawings for numerous k_2 values.

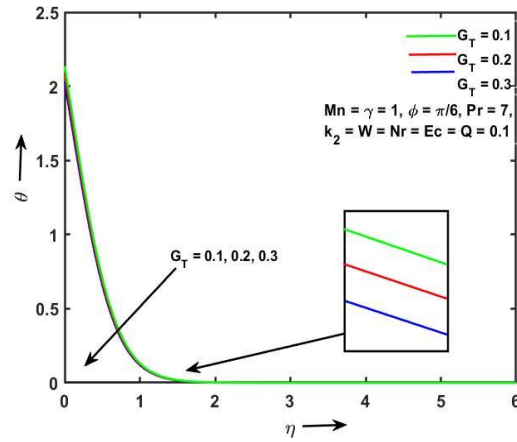


Figure 9. Temperature drawings for numerous G_T values.

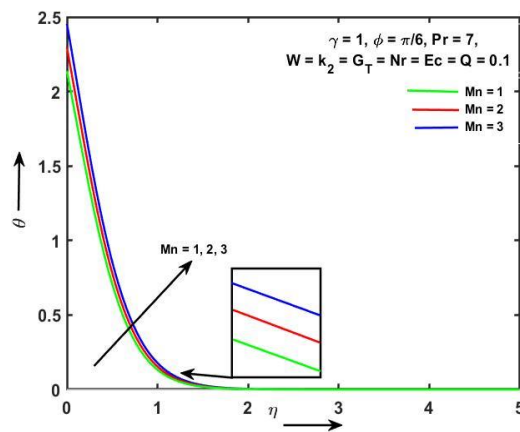


Figure 10. Temperature drawings for numerous Mn values.

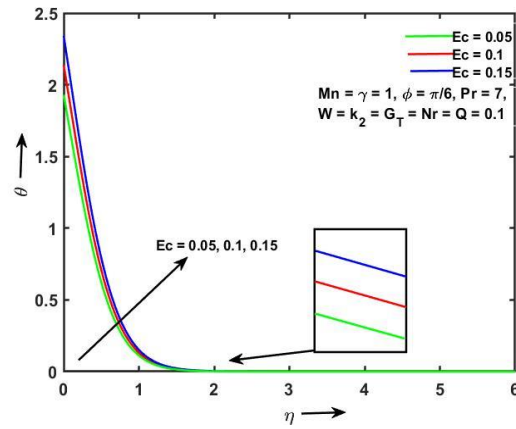


Figure 11. Temperature drawings for numerous Ec values.

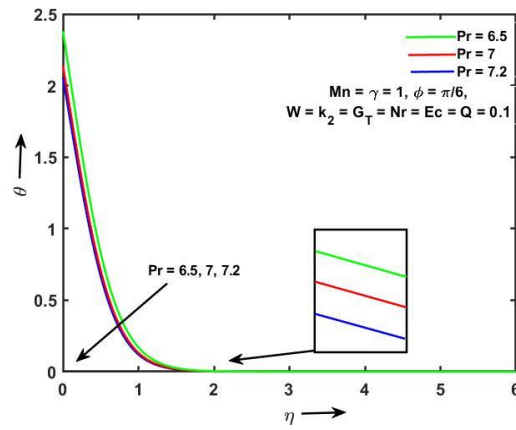


Figure 12. Temperature drawings for numerous Pr values.

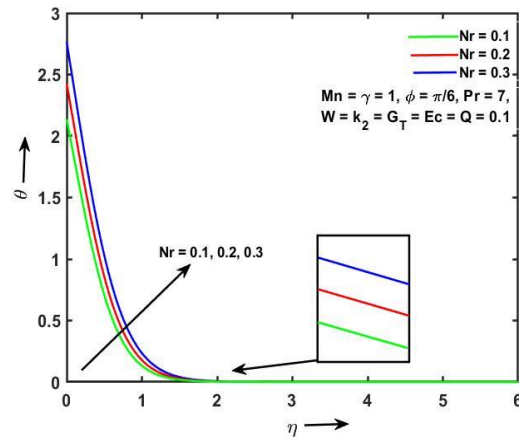


Figure 13. Temperature drawings for numerous Nr values.

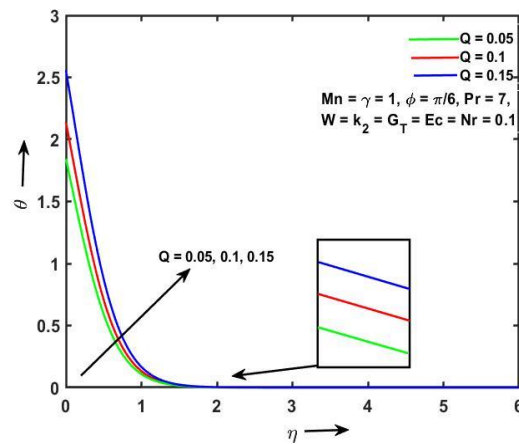


Figure 14. Temperature drawings for numerous Q values.

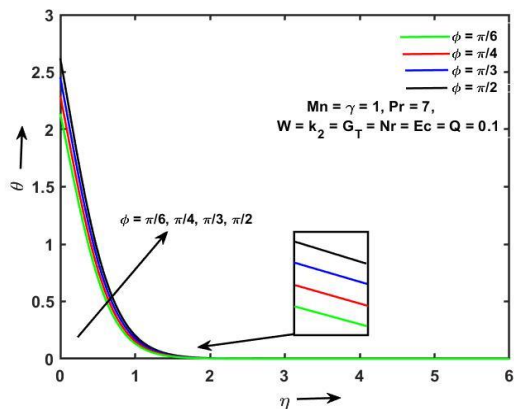


Figure 15. Temperature drawings for numerous ϕ values.

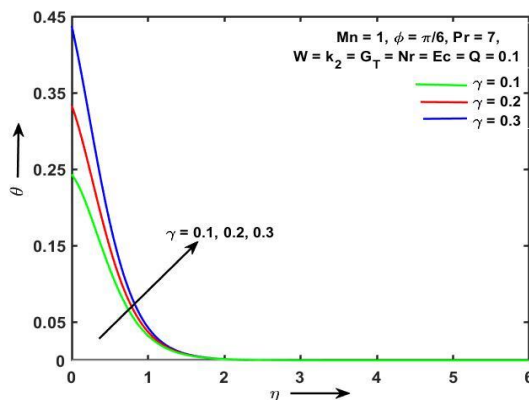


Figure 16. Temperature drawings for numerous γ values.

The temperature trends are illustrated in Figure 11 as the Eckert number Ec grows. It has been discovered that as the Eckert number climbs, so does the temperature profile. The Eckert number represents the relationship between kinetic energy and enthalpy in a flow. It depicts the labour required to convert kinetic energy into internal energy in the face of viscous fluid forces. The greater the Eckert number, the higher the fluid’s kinetic energy, resulting in more fluid vibration and more fluid-molecule collisions. Heat dissipation in the boundary layer region is aided by enhanced molecular collisions, increasing temperature profile. When the Eckert parameter is raised for Williamson fluid, the skin friction coefficient rises,

but the heat transfer coefficient falls. The surges temperature graph and the decreased volume fraction graph for the rising thermal radiation parameter are presented in Figure 13. Because the thermal boundary layer grows with N_r , the temperature also rises. When the thermal radiative parameter upsurges in the Williamson fluid, the skin friction coefficient upsurges but the heat transfer coefficient decreases. The outcome of the heat source parameter Q is seen in Figure 14. The heat source/sink serves as a heat producer. As the parameter estimations get more intensive, the fluid particles temperature rises. As an outcome, temperatures are rising. The skin friction coefficient grows as the Q parameter in the Williamson fluid is raised, while the heat transfer coefficient drops.

Figure 16 shows temperature curves for a variety of conjugate parameter amounts. The width of the boundary layer rises as it upsurges. When the conjugate parameter increases in the Williamson fluid, the skin friction coefficient increases but the heat transfer coefficient decreases. The numerical values of numerous physical characteristics, the skin-friction coefficient, and the Nusselt parameter are listed in Table 1.

Table 1. The skin-friction coefficient and heat transfer coefficient.

W	Mn	ϕ	G_T	k_2	Pr	Nr	Ec	Q	γ	$-\theta'(0)$	$C_f Re_s^{1/2}$	$Nu_s Re_s^{-1/2} = -\theta'(0)$
0.1										1.14257	-1.07730	3.13755
0.3	1	$\pi/6$	0.1	0.1	7	0.1	0.1	0.1	1	1.25762	-1.17854	3.20609
0.6										2.29706	-2.03324	3.44657
	1									1.14257	-1.07730	3.13755
0.1	2	$\pi/6$	0.1	0.1	7	0.1	0.1	0.1	1	1.25006	-1.17193	3.29394
	3									1.34994	-1.25882	3.45428
		$\pi/6$								1.14257	-1.07730	3.13755
		$\pi/4$								1.25006	-1.17193	3.29394
		$\pi/3$								1.34994	-1.25882	3.45428
		$\pi/2$								1.44364	-1.33944	3.61972
			0.1							1.14257	-1.07730	3.13755
			0.2							1.07991	-1.02160	3.08030
			0.3							1.02113	-0.96899	3.03010
				0.1						1.14257	-1.07730	3.13755
				0.5						1.3108	-1.22489	3.38959
				1						1.49734	-1.38524	3.72186
					6.5					1.13298	-1.06879	3.38033
					7					1.14257	-1.07730	3.13755
					7.2					1.14574	-1.08010	3.05693
						0.1				1.14257	-1.07730	3.13755
						0.2				1.13109	-1.06712	3.42785
						0.3				1.11761	-1.05516	3.76599
							0.05			1.14991	-1.08379	2.93021
							0.1			1.14257	-1.07730	3.13755
							0.15			1.13535	-1.07089	3.34178
								0.05		1.15275	-1.08631	2.84367
								0.1		1.14257	-1.07730	3.13755
								0.15		1.1281	-1.06447	3.55585
									0.1	1.20035	-1.12831	0.124327
									0.2	1.19758	-1.12587	0.26666
									0.3	1.19439	-1.12306	0.43119

Table 2 shows validation of the present result as well as previous outcomes.

The evaluation between the prior and current outcomes of $-\theta(0)$ and $-\theta'(0)$ for reformed amounts of Pr when $\phi = W = Mn = 0$ and $\gamma = 1$ and new parameter ($G_T, k_2, Nr, Ec,$ and Q) is also off in this validation.

Pr	-θ'(0)					-θ''(0)				
	Salleh et al. [17]	Arifin et al. [3]	Hashim et al. [8]	Goud et al. [7]	Current Research	Salleh et al. [17]	Arifin et al. [3]	Hashim et al. [8]	Goud et al. [7]	Current Research
3	6.0258	6.0513	6.05159	6.051715	6.05999	7.0258	7.0513	7.05159	7.051715	7.05999
5	1.7659	1.7604	1.76039	1.760392	1.76096	2.7659	2.7604	2.76039	2.760392	2.76096
7	1.1351	1.1168	1.11681	1.116814	1.11702	2.1351	2.1168	2.11681	2.116814	2.11702
10	0.7653	0.7645	0.76452	0.764524	0.76761	1.7653	1.7645	1.76452	1.764524	1.76761
100	0.1612	0.1478	0.14782	0.147801	0.1478	1.1612	1.1478	1.14782	1.147801	1.1478

5. Conclusions

The current study looked at a stretched surface of Williamson fluid with an aligned magnetic field and Newtonian heating. The effects of anti-Newtonian Williamson fluid parameter, magnetic impact, Prandtl parameter, permeability parameter, local temperature Grashof number, Eckert number, radiation parameter, aligned angle parameter, and heat source parameter on skin friction values, velocity, and temperature curves are numerically analysed. The following are some key points to consider:

- An increase in the amount of G_T increases to the momentum profiles and an increase in the amount of W, k_2, Mn and ϕ decline to the momentum profiles.
- An increase in $W, Mn, \phi, k_2, Nr, Ec, \gamma$ and Q upsurge to the temperature profiles, as well as an increment in G_T and Pr failure to the temperature profiles.
- As the physical parameters G_T, Nr, Ec, γ and Q rise, the skin-friction coefficient rises, but the inverse is true as W, Mn, k_2, Pr , and ϕ rise.
- The heat transfer coefficient (Nusselt number) increases as the physical parameters G_T and Pr increase, but the reverse impress increases as $W, Mn, k_2, Nr, Ec, Q, \gamma$ and ϕ grow.

References

- [1] K. Ahmad, Z. Wahid and Z. Hanouf, Heat transfer analysis for Casson fluid flow over stretching sheet with Newtonian heating and viscous dissipation, *Journal of Physics: Conference Series* 1127(1) (2019), 012028, IOP Publishing.
- [2] N. S. Arifin, S. M. Zokri, A. R. M. Kasim, M. Z. Salleh, N. F. Mohammad and W. N. S. W. Yusoff, Aligned magnetic field of two-phase mixed convection flow in dusty Casson fluid over a stretching sheet with Newtonian heating, *Journal of Physics: Conference Series*, IOP Publishing 890(1) (2017, September), 012001.
- [3] N. S. Arifin, S. M. Zokri, A. R. M. Kasim, M. Z. Salleh, W. N. S. W. Yusoff, N. F. Mohammad and S. Shafie, Aligned magnetic field on dusty Casson fluid over a stretching sheet with Newtonian heating, *Malaysian Journal of Fundamental and Applied Sciences*, 13(3) (2017), 245-248.
- [4] K. Y. Bing, A. Hussanan, M. K. A. Mohamed, N. M. Sarif, Z. Ismail and M. Z. Salleh, Thermal radiation effect on MHD flow and heat transfer of Williamson nanofluids over a stretching sheet with Newtonian heating, In *AIP Conference Proceedings* 1830(1) (2017), 020022. AIP Publishing LLC.
- [5] S. Das, A. Ali, R. N. Jana and O. D. Makinde, Magnetohydrodynamic boundary layer slip flow of radiating and chemically reactive nanofluid over a stretching sheet with Newtonian heating, *Journal of Nanofluids* 5(4) (2016), 606-616.
- [6] S. S. U. Devi and S. A. Devi, Numerical investigation of three-dimensional hybrid Cu-Al₂O₃/water nanofluid flow over a stretching sheet with effecting Lorentz force subject to Newtonian heating, *Canadian Journal of Physics* 94(5) (2016), 490-496.
- [7] B. S. Goud, Boundary layer and heat transfer Williamson fluid flow over a stretching sheet with Newtonian heating, *Turkish Journal of Computer and Mathematics Education (TURCOMAT)* 12(10) (2021), 1275-1280.
- [8] H. Hashim, M. K. A. Mohamed, N. Ishak, N. M. Sarif and M. Z. Salleh, Thermal radiation effect on MHD stagnation point flow of Williamson fluid over a stretching surface, In *Journal of Physics: Conference Series*, IOP Publishing 1366(1) (2019), 012011.
- [9] A. Hussanan, M. Z. Salleh, H. T. Alkasasbeh and I. Khan, MHD flow and heat transfer in a Casson fluid over a nonlinearly stretching sheet with Newtonian heating, *Heat transfer Research* 49(12) (2018).
- [10] I. Khan, M. Y. Malik, T. Salahuddin, M. Khan and K. U. Rehman, Homogenous-heterogeneous reactions in MHD flow of Powell-Eyring fluid over a stretching sheet with Newtonian heating, *Neural Computing and Applications* 30(11) (2018), 3581-3588.
- [11] J. K. Madhukesh, R. N. Kumar, R. P. Gowda, B. C. Prasannakumara, G. K. Ramesh, M. I. Khan and Y. M. Chu, Numerical simulation of AA7072-AA7075/water-based hybrid nanofluid flow over a curved stretching sheet with Newtonian heating: A non-Fourier heat flux model approach, *Journal of Molecular Liquids* 335 (2021), 116103.
- [12] M. K. A. Mohamed, M. Z. Salleh, R. Nazar and A. Ishak, Stagnation point flow over a stretching sheet with Newtonian heating, *Sains Malaysiana* 41(11) (2012), 1467-1473.

- [13] M. K. A. Mohamed, N. A. Ismail, N. Hashim, N. M. Shah and M. Z. Salleh, MHD slip flow and heat transfer on stagnation point of a magnetite (Fe_3O_4) ferrofluid towards a stretching sheet with Newtonian heating, *CFD Letters* 11(1) (2019), 17-27.
- [14] D. Qaiser, Z. Zheng and M. R. Khan, Numerical assessment of mixed convection flow of Walters-B nanofluid over a stretching surface with Newtonian heating and mass transfer, *Thermal Science and Engineering Progress* 22 (2021), 100801.
- [15] M. Qasim, I. Khan and S. Shafie, Heat transfer in a micropolar fluid over a stretching sheet with Newtonian heating, *Plos One* 8(4) (2013), e59393.
- [16] M. Ramzan and F. Yousaf, Boundary layer flow of three-dimensional viscoelastic nanofluid past a bi-directional stretching sheet with Newtonian heating, *AIP Advances* 5(5) (2015), 057132.
- [17] M. Z. Salleh, R. Nazar and I. Pop, Boundary layer flow and heat transfer over a stretching sheet with Newtonian heating, *Journal of the Taiwan Institute of Chemical Engineers* 41(6) (2010), 651-655.
- [18] N. M. Sarif, M. Z. Salleh and R. Nazar, Numerical solution of flow and heat transfer over a stretching sheet with Newtonian heating using the Keller box method, *Procedia Engineering* 53 (2013), 542-554.
- [19] I. Ullah, S. Shafie and I. Khan, Effects of slip condition and Newtonian heating on MHD flow of Casson fluid over a nonlinearly stretching sheet saturated in a porous medium, *Journal of King Saud University-Science* 29(2) (2017), 250-259.
- [20] M. Rahman, M. Khan and M. Manzur, Homogeneous-heterogeneous reactions in modified second grade fluid over a non-linear stretching sheet with Newtonian heating, *Results in Physics* 7 (2017), 4364-4370.